TECHNISCHE MECHANIK, 30, 1-3, (2010), 15 – 28
submitted: October 30, 2009

Numerical modelling of the microstructure effect on fatigue behaviour of Ni-base superalloys for turbine disk

G. Boittin, F. Gallerneau, D. Locq, P. Kanouté, G. Cailletaud

Nickel-based alloy like N18 can present various types of precipitate distributions according to the applied heat treatment. A model involving a three scale homogenization procedure is developed to characterize the influence of this microstructure on fatigue life. The microstructural parameters are the size and the volume fraction of the secondary and tertiary precipitates of γ' phase. Experimental results at 450 °C, specially designed to calibrate the model, allow to understand the role of tertiary precipitation. The first identification of the three scale homogenization model is shown.

1 Introduction

This article presents a physically based model describing fatigue behaviour of N18, a nickel-based powder metallurgy (PM) superalloy. This model takes into account some microstructural parameters such as size and volume fraction of the different populations of precipitates. The aim is to optimize heat treatments to improve the fatigue life of the component. As presented in Figure 1, the thermal field in the preform of the component is calculated, it is used as an input to evaluate the microstructural parameters. These parameters are introduced in a phenomenological model to evaluate the mechanical behaviour in each Gauss point of the component. A new mesh is necessary, to take into account the machining of the component from the preform. A mechanical finite element analysis (FEA) and a post processing calculation give the fatigue life prediction. They take as input the calculated, microstructure-dependent, mechanical behaviour. The challenge of this study is to build a model linking the microstructural parameters to the mechanical behaviour and the fatigue life (named "phenomenological model" in Figure 1). A first approach consisting of a multiscale analysis with a three scale homogenization model will be used to understand the effect of each microstructural parameter, before building the phenomenological model. The whole numerical procedure is implemented in the framework of ZSeT/ZeBuLoN, so that the computation of the thermal evolution inside the part during the heat treatment, the resulting microstructure and the response of the material during the mechanical tests are obtained in the same software. The paper is organised as follows. Microstructures of standard and tested N18 are described in section 2. Mechanical experimental results are shown in section 3. The effect of tertiary precipitates on tensile and LCF tests is exhibited. The microstuctural model is presented in section 4. The reader will successively find the description of the precipitate distribution, the precipitation model itself and its application to a turbine disk. Section 5 describes the general framework of the three scale homogenization model and a first application to a cyclic test.

2 Microstructure description

2.1 Microstructure of the standard subsolvus N18 superalloy

The N18 superalloy is constituted of two phases, a γ (FCC) matrix and the γ' precipitates (ordered cubic $L1_2$ structure), as shown in Figure 2. The precipitates are coherent with the matrix. They are classified into three categories depending on their size. The primary precipitates (1-4 μm) are intergranular. They are left unchanged by a subsolvus solutionning treatment. Indeed the grain boundaries are pinned by the primary intergranular precipitates in the case of a subsolvus heat treatment. During a supersolvus treatment, the primary γ' are dissolved, allowing grain growth. (That's why when the temperature of the solutionning treatment is below the γ'-solvus temperature,

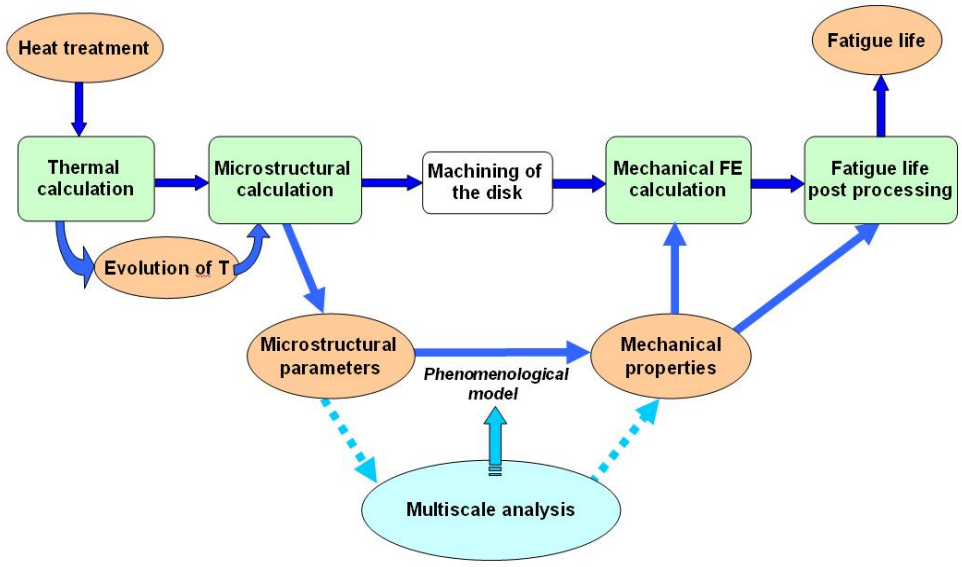

Figure 1: Methodology to model the influence of the heat treatment on the fatigue life.

the alloy presents a fine-grained microstructure (subsolvus), and, when the temperature is higher, a coarse-grained microstructure (supersolvus)). The secondary precipitates (γ'_{II}) appear at the beginning of the quench after the solutionning treatment, they are intragranular and cuboidal (200 nm). The tertiary γ' (γ'_{III}) are formed at the end of the quench, beetween the secondary precipitates. They are spherical to cuboidal and their diameter is less than 100 nm.

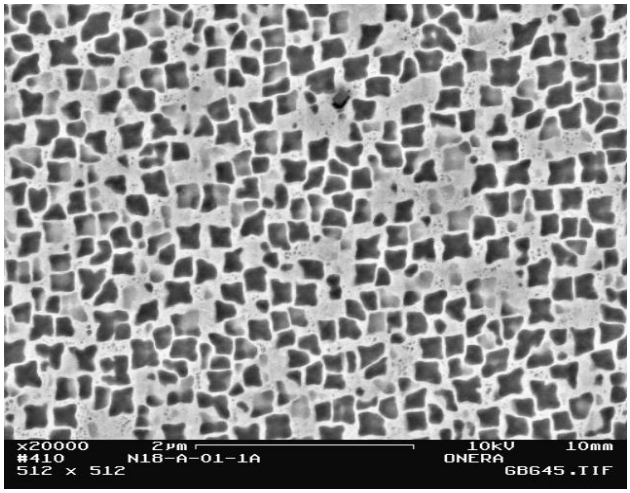

Figure 2: Microstructure of N18 after a supersolvus heat treatment and a standard ageing heat treatment 24 h at 700°C and 4h at 800°C (SEM).

An important scatter in fatigue life of fine-grained Ni-based PM superalloys is due to the presence of ceramic inclusions. The inclusions are then preferential sites for crack initiation because their size is larger (60 to 100 μ m) than the grain size (15 μ m for fine-grained N18). In order to prevent crack initiation on the inclusions, which hides microstructure effect, the mechanical tests of this study were performed on coarse-grained (60 μm, containing no primary precipitates) material at 450 °C.
The varying microstructural parameters are the size and volume fraction of the two populations of precipitates. Only the influence of tertiary γ' precipitates is described here. The influence of the secondary γ' will be described in a further paper.

2.2 Microstructure of the tested supersolvus N18 superalloy

The "standard" microstructure (Figure 3) is obtained after a supersolvus heat treatment and an air-quench followed by the standard double ageing treatment 700°C during 24 hours and 800°C during 4 hours. Figure 3-a shows a general SEM view, that exhibits mainly the secondary precipitates. The secondary γ' size is about 180 nm and the tertiary about 20 nm, as demonstrated in the TEM image in Figure 3-b.

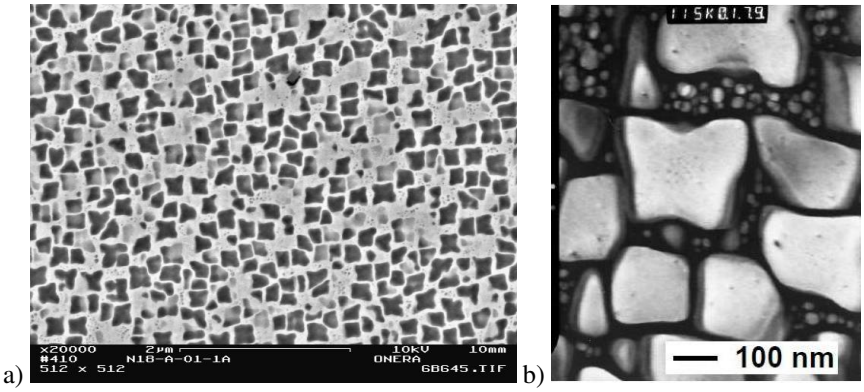

a) b)

Figure 3: Microstructure of N18 obtained after a supersolvus heat treatment and an air-quench followed by the standard double ageing treatment 700°C during 24 hours and 800°C during 4 hours. a) General view of a 4 μm x 3 μm zone showing spatial distribution of secondary precipitates (SEM). b) Zoom showing the population of tertiary precipitates between the secondary precipitates (TEM).

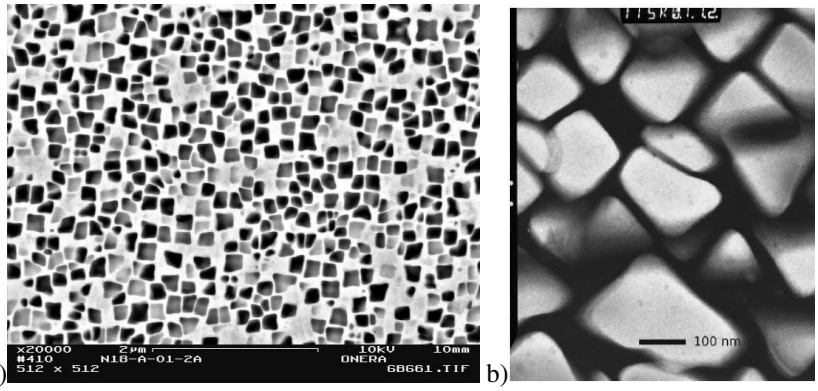

a) b)

Figure 4: Microstructure of N18 obtained after a supersolvus heat treatment and an air-quench followed by the ageing treatment 900°C during 1 hour. a) General view of a 4 μm x 3 μm zone showing spatial distribution of secondary precipitates (SEM). b) Zoom showing the absence of the population of tertiary precipitates between the secondary precipitates (TEM).

The microstructure without tertiary γ' precipitates is obtained after a supersolvus heat treatment and an air-quench followed by an ageing at 900°C during 1 hour. The figure 4-a presents a general SEM view very similar to the SEM image of the standard microstructure (Figure 3-a). The secondary γ' size is about 180 nm. But the tertiary γ' have been almost totally dissolved, as observed in Figure 4-b. Topologically Closed Packed (TCP) precipitates are observed at some grains boundaries. As these particles are very fine and only some boundaries are affected, it is assumed that TCP phases have no influence on the mechanical behaviour.

The size and volume fraction of the secondary γ' were determined using image analysis on Scanning Electron Microscopy (SEM) images (back-scattered electrons). The size of the tertiary γ' were determined through Transmission Electron Microscopy (TEM) images. After the mechanical tests, the rupture surfaces of the specimens were studied by SEM.

3 Experimental results

3.1 Experimental procedure

The test specimens were taken from an as-forged part supplied by SNECMA. Cylinders of 12 mm in diameter were extracted and heat treated. Then a specimen was machined from the cylinder and tested at 450°C under the conditions described in Table 1. One test has been performed for each microstructure.

Except for the monotonic tension test on the specimen with the microstructure without tertiary precipitates, all the tests were performed with a prescribed strain rate of $10^{-3}s^{-1}$. The stress represented on the Figures is normalized.

Test 1	Tensile test
Test 2	Repeated LCF test $R_\varepsilon = 0$, $\varepsilon_{max} = \varepsilon_1$
Test 3	Repeated LCF test $R_\varepsilon = 0$, $\varepsilon_{max} = \varepsilon_2$
Test 4	Total reverse Incremental LCF test $R_\varepsilon = -1$, three strain levels ε_3, ε_4, ε_5.

Table 1: Test matrix, $R_\varepsilon = \varepsilon_{min}/\varepsilon_{max}$, the tests were performed at 450°C.

3.2 Tensile tests

The instabilities observed on the curves recorded during the tensile test of supersolvus N18 (Figure 5) are related to Portevin-Le Chatelier effect. This effect is very weak (only one peak) in the case of the microstructure without tertiary γ'. The instabilities begin for a strain of 1%, which is higher than the maximum strain defined in the fatigue tests, and their amplitudes remain small. So, it is assumed that the Portevin-Le Chatelier effect has little influence on the fatigue test results.

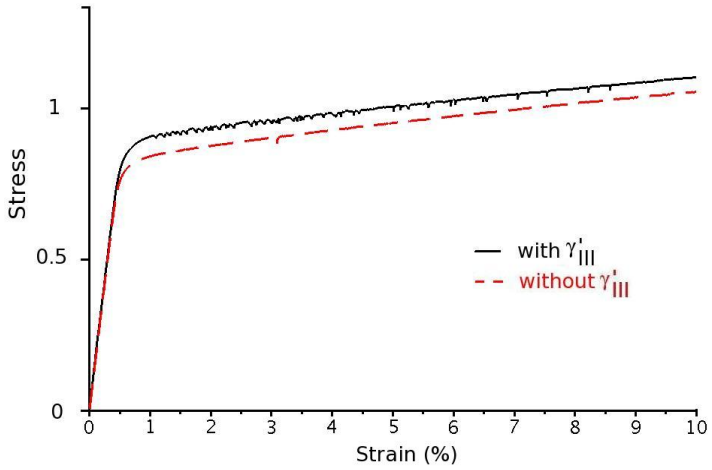

Figure 5: Influence of the tertiary γ' precipitates on the tension behaviour of supersolvus N18 at 450°C.

The tertiary precipitates have influence neither on the Young modulus nor on the hardening modulus. But the microstructure with tertiary precipitates shows a higher 0.2% yield stress than the microstructure without tertiary precipitates. The Ultimate Tensile Stress (UTS) of both materials is almost identical. Schirra et al. (2004) conducted tests on two powder metallurgy superalloys (KM4 et SR3). They reported no influence of the tertiary on the UTS, as we observed. But contrary to our results, they observed no effect of the tertiary precipitates on the yield stress. On IN100 alloy, Milligan et al. (2004) found an influence of the tertiary precipitates on the yield

stress according to the rule $L0 + Cd_3^{1/2}$, with d_3 the size of tertiary precipitates and C a multiplicative factor. The exponent 1/2 comes from the weak pair-coupling cutting of tertiary precipitates (cf eq. 9).

3.3 Fatigue tests

The stabilized loops (of tests 2 and 3) of the specimens with the microstructure without tertiary precipitates present the same amplitude as the stabilized cycles of the specimens with the "standard" microstructure, but a lower mean stress (Figures 6 and 7).
The fatigue loop of both specimens are almost elastic: very little cyclic plasticity is observed after the first cycles. The steady state of the specimen without tertiary γ' presents a plastic strain larger than the standard one for the test 3.

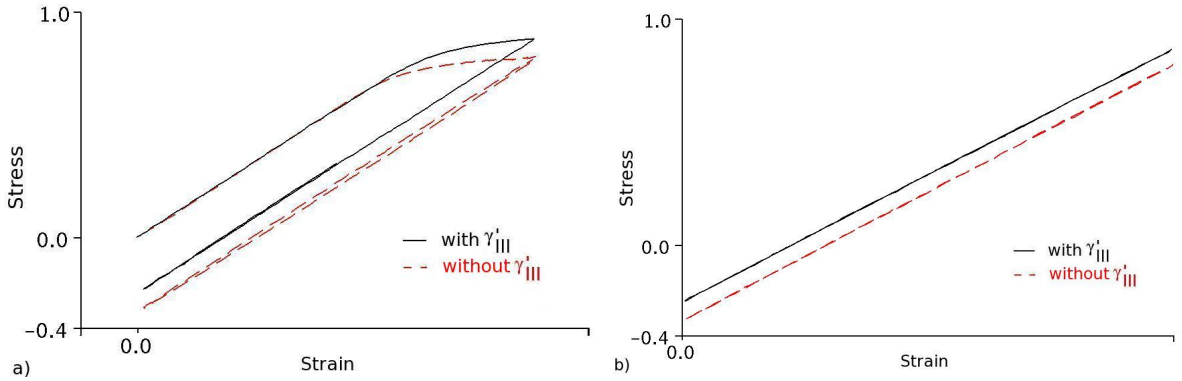

Figure 6: Initial (a) and stabilized (b) cycles of specimens submitted to LCF test 2 with the standard supersolvus microstructure (continuous line) and supersolvus without tertiary (dashed line).

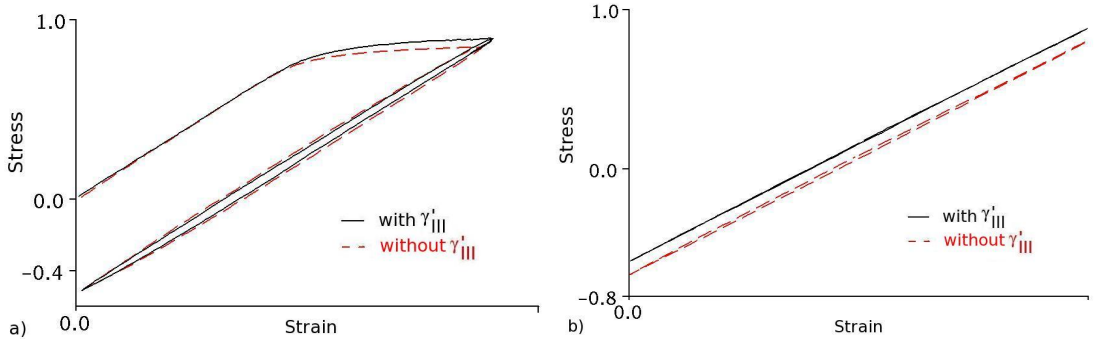

Figure 7: Initial (a) and stabilized (b) cycle of specimens submitted to LCF test 3 strain with the standard supersolvus microstructure (continuous line) and supersolvus without tertiary (dashed line).

An important cyclic hardening was observed in the N18 superalloy (Sansoz (2000)). The incremental fatigue test is designed to obtain the cyclic hardening curve for the different microstructures. Both microstructures show the same strong cyclic hardening, as observed in Figure 8.

3.4 Fractographies for the study of crack initiation

No inclusions or coarse pores were observed on the fractographies. The crack must have initiated "on the microstructure" itself, as expected. Several crack initiations on a large facet perpendicular to the tension axis at or near the surface of the specimen can be observed on Figures 9 and 10. The crack path is very tortuous, and along

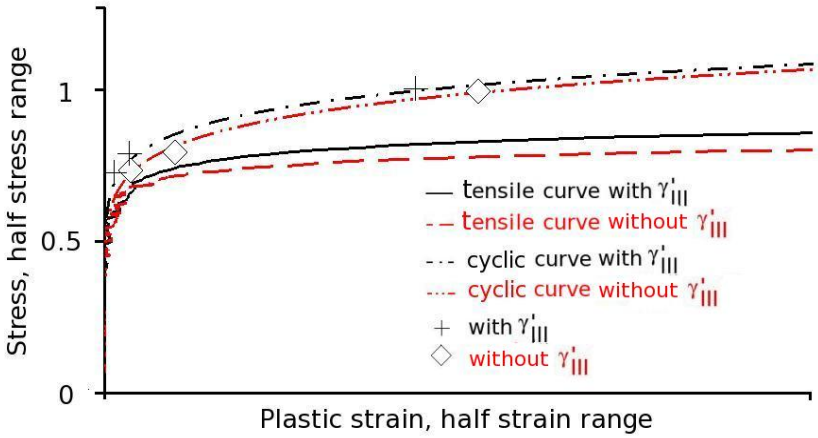

Figure 8: Monotonic and cyclic hardening curves of N18 at 450°C.

facets, which indicates a mainly transgranular crack propagation for both specimens, independently of the tests conditions.

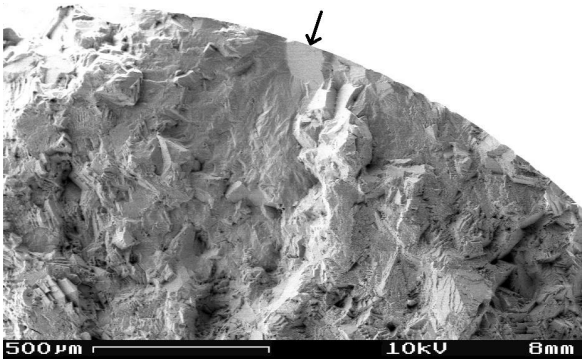

Figure 9: Fractography of a crack initiation of the specimen submitted to LCF test 3 with the supersolvus standard microstructure.

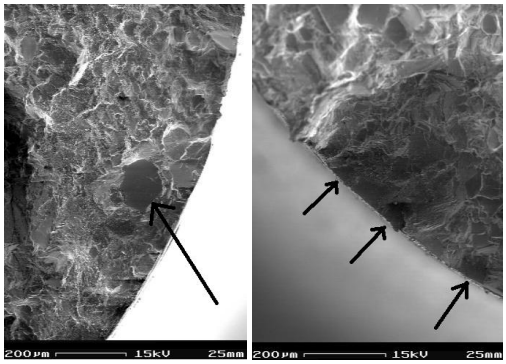

Figure 10: Fractographies of the crack initiations of the specimen submitted to incremental LCF test 4 with the supersolvus standard microstructure.

3.5 Discussion

Two types of hardening are usually chosen to model the behaviour of the material: isotropic hardening, which enlarges the elasticity domain in the stress space and kinematic hardening, which translates this domain. A good balance between these phenomena is necessary to predict the stabilized cycle amplitude and the mean stress, that

represent critical inputs for the fatigue life prediction models. In Figure 12, the curves with continuous and dashed line represent the tension curves and the dashed-dotted lines represent the stress minus the strain multiplied by Young's modulus divided by two ($\sigma - E\varepsilon/2$), which corresponds to the mean stress of the first cycle in the case of a totally elastic unloading. As the dashed-dotted-line curve is in a quite good agreement with the experimental points, the lower mean stress of the microstructure without tertiary γ' is mainly due to its lower yield stress.

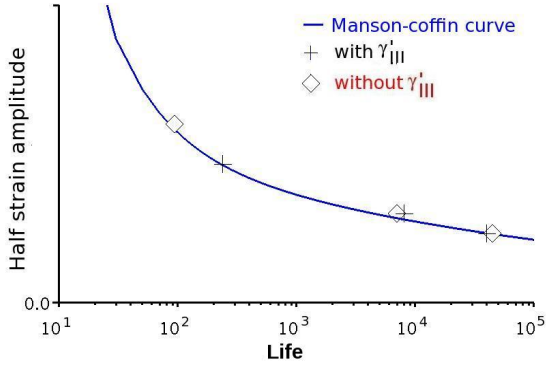

Figure 11: Manson-Coffin curve of N18 coarse grain at 450 °C.

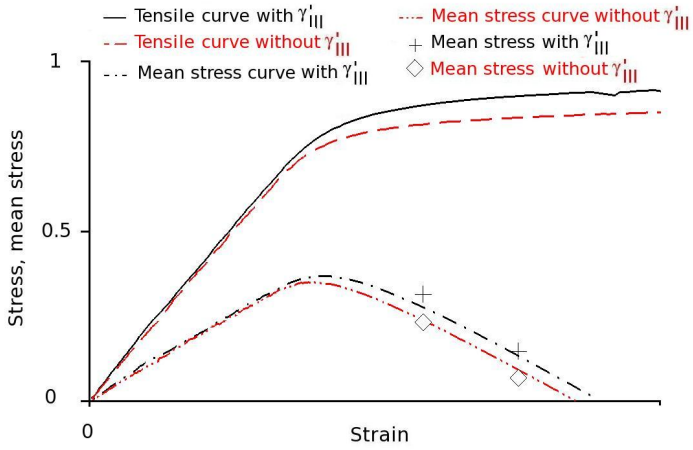

Figure 12: Relaxation of the mean stress. Continuous and dashed line: tension curve. Dashed-dotted line: $\sigma - \varepsilon E/2$. Symbols: mean stress measured on the LCF tests 2 and 3.

As a lower mean stress is beneficial for the life at given stress and strain amplitudes, we could expect a larger life for the test specimens of microstructure without tertiary precipitates, but only small differences are observed between the life of the two microstructures as shown in Figure 11. The life of the specimen with the microstructure without tertiary was 12% shorter than the life of specimen with the standard microstructure, for the test 3 but inversely for the test 2. The microstructure without tertiary precipitates is probably less resistant to crack initiation, which decreases the fatigue life, but its lower mean stress balances this decrease.
Runkle and Pelloux (1979) showed that in Astroloy, the dissolution of tertiary precipitates (and primary ones which implies grain growth) induces a reduction of the life up to 33% at 423°C for a strain range of 2.2% and a frequency of 0.05 Hz. They thought that the presence of tertiary precipitates delays the crack initiation in stage I, which is especially useful at relatively low temperature till 500°C. The present results show that the reduction in fatigue life is probably mainly related to grain growth, but the dissolution of tertiary γ' may also have a small influence.
Schirra et al. (2004) showed that for KM4 and SR3 superalloys, the decrease of the size of the tertiary precipitates had a positive effect on the fatigue life till crack initiation but a negative effect on crack propagation.

4 Modelling the microstructure

4.1 Model of precipitation

The influence of the cooling rate during the quenching operation of N18 alloy was described and modelled by Milhet-Gayraud (1994). Following observations can be noted in this study:
- the nucleation of γ' precipitates is correctly described by homogeneous nucleation,
- their coarsening could be described with LSW model (Lifshitz, Slyozov, Wagner),
- it is not necessary to account for growth in the model.
On the other hand, models involving nucleation, growth and coarsening have been proposed by Gabb et al. (2000) and Jou et al. (2004) and implemented in the PrecipiCalc software for multicomponent systems.

In the case of an homogeneous nucleation, the nuclei are homogeneously distributed in the material. There is no effect of the grain boundary and the precipitation takes place as in an "infinite" grain.
The total variation of the free energy (ΔG) due to the creation of a nucleus has three origins:
- the creation of a volume V of γ' phase, which decreases the free energy by $V\Delta G_v$ (ΔG_v volume nucleation energy),
- the creation of an interface S between γ and γ' phases, which increases the free energy by $S\sigma$ (σ interfacial energy),
- the lattice misfit between the two phases, which increases the free energy by a strain energy $V\Delta G_d$.
Considering that nuclei are spheres of radius r, the free energy variation is:

$$\Delta G = -\frac{4}{3}\pi r^3(\Delta G_v - \Delta G_d) + 4\pi r^2\sigma \tag{1}$$

The lattice misfit between the two phases is neglected in a first approach.

The nucleation rate, J_n, is the product of the number of nucleated particles per unit of time by the probability that the nucleus will grow. The number of nucleated particles is given by Boltzmann statistics. An additional factor Z (Zeldovich factor, $Z = (\Delta G^*/3\pi k_B T)^{-1/2}$) is introduced to take into account the probability that a nucleus of a size bigger than the critical one is dissolved. The nucleation rate is then:

$$J_n = \frac{18D}{d_m^4 R^*}\left(\frac{\Delta G^*}{3\pi k_B T}\right)^{1/2} exp\left(-\frac{\Delta G^*}{k_B T}\right) \tag{2}$$

where ΔG^*, barrier of nucleation, R^*, the critical radius, and D the diffusion coefficient, are respectively:

$$\Delta G^* = \frac{4}{3}\pi\sigma R^{*2} \qquad R^* = 2\frac{\sigma V_m}{\Delta G_p} \qquad D = D_0 exp\left(\frac{-E_a}{R_g T}\right) \tag{3}$$

and where d_m is the lattice parameter of the γ' phase.

Lifshitz, Slyozov (1961) and Wagner (1961) have independently developed a theory of coarsening kinetics in a binary system. In their approach, the rate of coarsening of the precipitate is given by:

$$\frac{dR_i}{dt} = \frac{2d_0 D}{R_i^2}\left(\frac{R_i}{R_c^*} - 1\right), \qquad \text{with} \qquad d_0 = \frac{2\sigma c_e V_m}{c_p^2 R_g T} \tag{4}$$

where d_0 is the capillary length, and R_c^* is the critical radius of coarsening, defined by:

$$R_c^* = 2d_0\frac{c_p - c_e}{c_m - c_e} \tag{5}$$

where V_m is the molar volume, c_m and c_p are the concentrations of γ'-forming elements in the matrix and the

precipitates respectively.

The equation defining the evolution of the number of precipitates is:

$$\frac{\delta N_R}{\delta t} = -\frac{\delta}{\delta R}(N_R \frac{\delta R}{\delta t}) + j \tag{6}$$

where j is the source term corresponding to the nucleation of the precipitates (j is different from zero only for $R = R^*$).

4.1.1 Calibration and validation of the model

The calibration was made as follows: c_e is calculated to fit the dissolution curve (Milhet-Gayraud (1994)), σ is chosen according to the early precipitation at a cooling rate of 180°C/min (Milhet-Gayraud (1994)), ΔG and Vm are taken from the literature (Wendt and Haasen (1983)), as well as D (Flageolet (2005)).
Table 2 shows the results calculated by the model compared to the experimental results. The model delivers a rather good size of the secondary precipitates, a good approximation of the size of the tertiary precipitates. Only the volume fraction of the tertiary precipitates is a little underestimated.

	experimental				calculation			
heat treatment	fp2	t2	fp3	t3	fp2	t2	fp3	t3
20 K/min	-	200-300	-	5-50	36.8%	368	0.6%	27
180 K/min	-	100-250	-	10-30	36.4%	127	0,04%	8
1000 K/min	-	25-85	-	x	44.7%	64	0%	x
10200 K/min	-	20-25	-	x	42.4%	27	0%	x
2 stages quench*	-	700(oct) 300	-	40	29%	220	9.3%	50
standard cycle	35	200	10	50	37.9%	170	5.3%	24

Table 2: Comparison of the experimental results (Milhet-Gayraud (1994), *Nazé (2005)) and the calculation, (oct means octocube). fp2, fp3 are the volume fractions of the secondary and tertiary precipitates respectively. t2, t3 are the sizes of the secondary and tertiary precipitates respectively.

4.2 Modelling of the microstructure variation in a disk

The mesh shown in Figure 13 presents the preform of a disk just after forging. A thermal calculation has been made to compute the temperature field during an air quench. The temperature history is then used to compute the microstructure evolution. The structure is axisymmetric. As it is supposed symmetric with respect to r axis, only one half of the disk is represented. Figure 13-a shows the contour of the γ' volume fraction during the quenching operation. Due to the higher cooling rate, the amount of γ' is a little larger near the surface, nevertheless, the difference remains low (minimum 0.452; maximum 0.494). A much bigger difference is observed on the size distribution (Figure 13-b). This effect is illustrated by means of curves at the points A near the surface, and B in the core of the disk. The unit on the y-axis is the volume fraction of each class divided by the size of the class (dr is the difference between the maximum and the minimum radius of the class of sizes). So, the integration of each peak gives the volume fraction of the precipitates. As expected, the microstructure near the surface (A) shows no significant volume fraction of tertiary precipitates and the secondary precipitates are finer than the microstructure deep below the surface (B). Similar results were already experimentally observed by Wlodek et al. (1992) and Hochstetter (1994) in the N18 superalloy.

5 Modelling the influence of the microstructure on the mechanical behaviour

The model should be able to determine the role of the microstructural parameters:
- secondary precipitate size,
- tertiary precipitate size,
- volume fraction of the secondary precipitates,

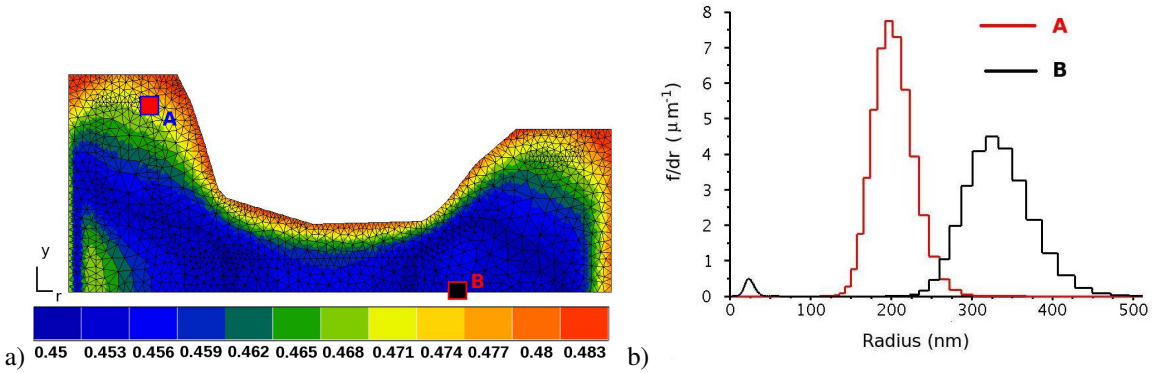

Figure 13: Volume fraction of γ' precipitates inside 1/2 disk during the quench. a) Contour of the γ' volume fraction, b) γ' size distribution for a point near the surface (A) and in the core of the disk (B) after treatment.

- volume fraction of the tertiary precipitates.

5.1 Model

As described in the article of Roos et al. (2004) for TiAl alloys, it is possible to imbricate TFA (Transformation Field Analysis) homogenization models at different scales to model the influence of different phases on the macroscopic behaviour. In N18 superalloy, as the mean size of the grains is about 60 micrometers and the size of the precipitates is either 200 nanometers for the secondary γ' or 20 nanometers for the tertiary γ', it is then possible to separate the three homogenization scales. The first scale of the model deals with the homogenization of the matrix and the tertiary precipitates. Each of the two constituents is given a law according to a viscoplastic crystal plasticity model (Meric et al. (1991)), whose equations are given in Table 3. The octahedral and cubic slip systems are considered to be activated for γ/γ' superalloys. The result of the first homogenization will be named "homogenized matrix". The second scale concerns the homogenization of the "homogenized matrix" with the secondary precipitates. The law chosen for the secondary precipitates follows the same model. The result of this homogenization is named "monograin". The third scale is the polycrystal scale. A polycrystal of 25 grains is computed. The same kind of TFA self-consistent homogenization is used for the two lower scales and a FEA or a TFA self-consistent scheme is used for the polycrystal homogenization. The polycrystal is described by 25 grains with different orientations and the same volume. Figure 14 gives a visual summary of the numerical procedure.

This approach requires to know the crystalline behaviour of the three constituents (matrix, secondary and tertiary precipitates). The crystalline behaviour of the secondary γ' can be identified, knowing the crystalline behaviour of the matrix and the macroscopic behaviour of a polycrystal made up of only the matrix and the secondary γ' (i.e. a microstructure without tertiary precipitates). The beginning of the identification for the of the crystalline behaviours of the matrix and of the secondary precipitates is presented in section 5.2 Then the behaviour of the tertiary γ' can be identified from the macroscopic behaviour of a polycrystal containing the two types of precipitates.

In the case of an homogenization with a self-consistent scheme, the volume fraction and the shape of the particle is taken into account, but not the size of the particle. The influence of the size of the precipitates is then explicitly introduced in the hardening rules of the crystal plasticity model.

5.2 First calibration of the model : elasticity and plastic threshold for N18 with a microstructure without tertiary precipitates

The elasticity in the two phases has a cubic form. It was reported that the difference between the elasticity coefficients of the γ' precipitates and the γ matrix is in the range of 10%, for a wide range of γ/γ' superalloys. Data from Espie (1996) concerning the elastic moduli of the matrix of AM1 single crystal at 20 and 650°C are used. To estimate the elastic constants of the matrix of N18 at 450°C, a linear interpolation of the coefficients of the AM1

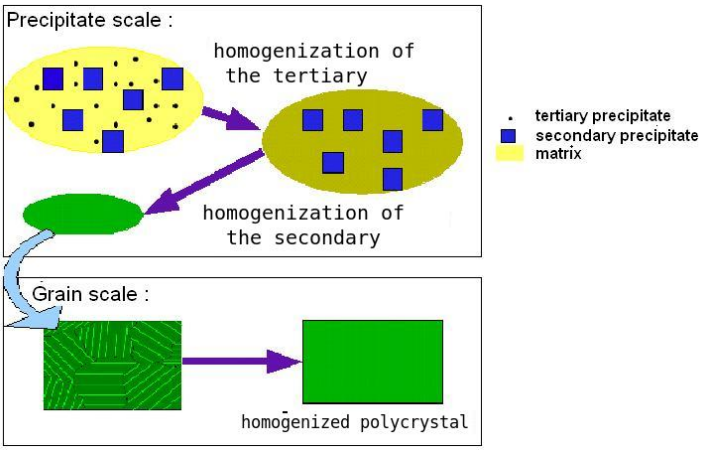

Figure 14: Three scale homogenization model.

$$\dot{\gamma_s} = \left\langle \frac{|\tau^s - x^s| - r^s}{K} \right\rangle^n sign(\tau^s - x^s)$$

$$\dot{x}^s = C\dot{\gamma}^s - D\dot{v}^s x^s$$

$$r^s = R_0 + \Sigma_r h^{sr} Q^r (1 - e^{-b^r v^r})$$

$$\dot{v}^s = |\dot{\gamma}^s|$$

x^s is the kinematic hardening, r^s the isotropic hardening and $\dot{\gamma}^s$ the plastic flow rate, on slip system s.

$<>$ is the function: positive part.

Table 3: Equations of the Meric-Cailletaud's model (Meric et al. (1991)).

matrix at 20 and 650°C was chosen. The elastic coefficients of the secondary γ' were chosen to fit the experimental curve.

The plastic behaviour of each phase is not well known. Some works were done on single crystals by Espie (1996); Nitz and Nembach (1999); Gaubert (2009). They show that octahedral and cubic slip systems are active in these alloys. The Critical Resolved Shear Stress (CRSS) (the coefficient R_0 in the equations of Table 3) found for the matrix alone by Espie (1996), is very low (90 MPa). It is incompatible with the plastic threshold observed on the polycrystal (the CRSS should be more than 400 MPa). This difference is due to the presence of precipitates, which pinned the dislocations and delay plasticity. Orowan's stress necessary to bypass the precipitates according to Kocks formula (Kocks (1977)), is:

$$\tau_{OR} = 0.9 \frac{[ln(2\pi r/b)]^{3/2}}{[ln(L/b)]^{1/2}} \left(\frac{K_{edge}}{b(L - (\pi/2)r)} \right) \tag{7}$$

with $K_{edge} = \dfrac{Gb^2}{2\pi(1-\nu)}$

With a Burgers vector b of $2.5.10^{-10}$ m (Heilmaier et al. (2001)), L=244 nm (corresponding to the length between the center of cubes of 200 nm, in a material with a γ' volume fraction of 0.45), a shear modulus G of 100 GPa, and a radius r of 100 nm (the half of the length of the cube), a first estimation of the Orowan stress is 490 MPa.

For strong pair-coupling cutting of the precipitates, the critical resolved shear stress (CRSS) τ_{HR} would be, ac-

cording to Huther and Reppich (1978):

$$\tau_{HR} = 0.415 \frac{T_L w f^{1/2}}{br} \left(\frac{\pi^2 r \gamma_{APB}}{4 w T_L} - 1 \right)^{1/2} \left(0.94 (1 + C_{SL} \frac{f^{1/2}}{2}) \right) \tag{8}$$

For weak pair-coupling cutting of the precipitates, the critical stress τ_{SL} would be, according to Reppich (1993):

$$\tau_{SL} = \frac{\gamma_{APB}}{2b} \left(A1 \left(\frac{\gamma_{APB} r f}{T_L} \right)^{1/2} - A2 f \right) (1 + C_{SL} \eta_{SL}) \tag{9}$$

with w=3.34 a parameter accounting for the elastic repulsion of the dislocation within the precipitates, C_{SL}=1, $T_L = Gb^2/2$ and an antiphase boundary energy of $\gamma_{APB} = 0.14\ J.m^{-2}$ (these values were taken in Heilmaier et al. (2001)), τ_{HR} is equal to 220 MPa and τ_{SL} is equal to 700 MPa. τ_{HR} is below the Orowan stress and the CRSS of weakly coupled dislocations, so the precipitates are sheared by strongly coupled dislocations, which is confirmed by more accurate discrete dislocation dynamics computation done for AM1 alloy at 1000K (Vattré et al. (2009)), and by experiment on N18 alloy at 700°C (Flageolet (2005)) and on IN100 alloy at room temperature (Heilmaier et al. (2001); Shenoy et al. (2008)). So neither the matrix nor the precipitates could be sheared until the stress reaches the value of $\tau_{HR} + \tau_{SS}$, τ_{SS} is the solution strengthening stress, it is the value of the CRSS of the matrix alone. Then, shearing of the precipitates by strongly coupled dislocations occurs. It is justified to give to the matrix and to the precipitates the same CRSS, $\tau_{HR} + \tau_{SS}$, as the dislocations can not move in the matrix until stress reaches this value and the precipitates are sheared above this value. So the coefficient R_0 (Table 3) of the crystalline laws of both constituents is the same.
The antiphase boundary energy is difficult to compute accurately and has a large influence on the CRSS. As it is difficult to obtain an accurate value from the literature, the CRSS was determined experimentally to fit the observed macroscopic plastic threshold stress. A value of 430 MPa was found, which leads to τ_{HR} = 340 MPa. This corresponds, for example, to a shear modulus of 100 GPa and an antiphase boundary energy of 0.272 $J.m^{-2}$.

5.3 First calculation for a microstructure without tertiary precipitates

The matrix was reported to show an almost perfect plastic behaviour. So, no isotropic hardening was introduced in the model but a small kinematic hardening was used ($Q^r = 0$ and $x^s \neq 0$ for all the slip systems in the matrix). Since the polycrystal of N18 alloy exhibits isotropic and kinematic hardening, both of them were introduced in the behaviour of the precipitate ($Q^r \neq 0$ and $x^s \neq 0$ for all the slip systems in the secondary precipitates). The results of the calculation compared to the experimental fatigue test 3 is presented in Figure 15. The interactions between slip systems were limited to self hardening, no latent hardening was introduced. The identified plastic threshold is accurate but an improved description of the hardening is currently developed.

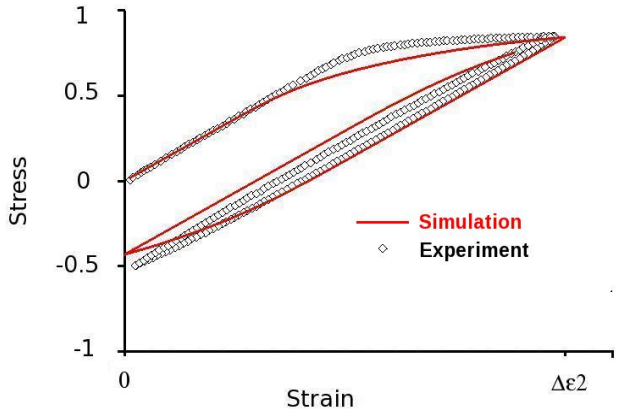

Figure 15: Comparison between experiment and numerical simulation for the first cycle of the test 3, at 450°C.

6 Conclusions and perspectives

A numerical procedure devoted to the prediction of the microstructure of the N18 alloy during heat treatments was implemented and validated in the software ZSeT/ZeBuLoN. It provides the size and volume fraction of the different types of γ' precipitates. A three scale model describing the effect of the microstructure on fatigue life is proposed. The influence of the tertiary precipitates was first studied. In repeated fatigue tests, the specimens with a microstructure without tertiary precipitates have a lower yield stress and their stabilized loops have a lower mean stress than the ones of the microstructure with tertiary precipitates. Nevertheless, almost no difference is observed in the fatigue life resistance of the two microstructures. A model taking into account the tertiary and the secondary γ' precipitates is being developed. Computational tests with various conditions and microstructures will then be achieved. From these tests, a macroscopical behaviour of the polycrystal depending on the microstructural parameters will be deduced. The tool developed to compute microstructure will allow to calculate the microstructure variation in a disk and the resulting life duration through a finite element calculation applying the macroscopic model.

7 Aknowlegment

SNECMA is gratefully thanked for their support in giving the as-forged part.

References

Espie, L.: *Etude experimentale et modelisation numerique du comportement mecanique de monocristaux de superalliages*. Ph.D. thesis, Ecole nationale Superieure des Mines de Paris (1996).

Flageolet, B.: *Effet du veillissement du superalliage base nickel N18 pour disques de turbines sur sa durabilité en fatigue et en fatigue fluage à 700° C*. Ph.D. thesis, Université de Poitiers (2005).

Gabb, T. P.; Backman, D. G.; Wei, D. Y.; Mourer, D. P.; Furrer, D.; Garg, A.; Ellis, D. L.: γ' formation in a nickel-base disk superalloy. In: T. M. Pollock; R. D. Kissinger; R. R. Bowman; K. A. Green; M. McLean; S. L. Olson; J. J. Schirra, eds., *Proceedings of Superalloys 2000*, pages 405–414, TMS Warrendale USA (2000).

Gaubert, A.: *Modélisation des effets de la évolution microstructurale sur le comportement mécanique du superalliage monocristallin AM1*. Ph.D. thesis, Mines-ParisTech (2009).

Heilmaier, M.; Leetz, U.; Reppich, B.: Order strengthening in the cast nickel-based superalloy IN100 at room temperature. *Materials Science and Engineering A*, 319-321, (2001), 375–378.

Hochstetter, G.: *Propagation des fissures a hautes temperatures dans le superalliage N18 pour disques de turbomachine. Interactions entre la nature des sollicitations mecaniques et des effets d'oxydation*. Ph.D. thesis, École Nationale Supérieure des Mines de Paris (1994).

Huther, W.; Reppich, B.: Interaction of dislocations with coherent, stress-free, ordered particles. *Z. fuer Metallkunde*, 69, (1978), 628–634.

Jou, H.; Voorhees, P.; Olson, G. B.: Computer simulations for the prediction of the microstructure/property variation in aeroturbine disks. In: K. A. Green; T. M. Pollock; H. Harada; T. E. Howson; R. C. Reed; J. J. Schirra; S. Walston, eds., *Proceedings of Superalloys 2004*, pages 877–886, TMS Warrendale USA (2004).

Kocks, U.: The theory of an obstacle-controlled yield strength - report after an international workshop. *Materials Science and Engineering*, 27, (1977), 291.

Meric, L.; Poubanne, P.; Cailletaud, G.: Single crystal modeling for structural calculations: Part 1 - Model Presentation. *J. Engng. Mat. Technol.*, 113, (1991), 162–170.

Milhet-Gayraud, N.: *Etude experimentale et modelisation de la precipitation γ' dans le superalliage N18*. Ph.D. thesis, Institut National Polytechnique de Grenoble (1994).

Milligan, W.; Orth, E.; Schirra, J.; Savage, M.: Effects of microstructure on the high temperature constitutive behavior of IN 100. In: K. A. Green; T. M. Pollock; H. Harada; T. E. Howson; R. C. Reed; J. J. Schirra; S. Walston, eds., *Proceedings of Superalloys 2004*, pages 331–339, TMS Warrendale USA (2004).

Nazé, L.: unpublished data (2005), centre des Matériaux.

Nitz, A.; Nembach, E.: Critical resolved shear stress anomalies of the $l1_2$-long-range ordered γ' phase of the superalloy NIMONIC 105. *Materials Science and Engineering A*, 263, (1999), 15–22.

Reppich, B.: Particle strengthening. In: H. Cahn; et al., eds., *Materials Science and Technology*, vol. 6 (1993).

Roos, A.; Chaboche, J.; Gelebart, L.; Crepin, J.: Multiscale modelling of titanium aluminides. *Int. J. Plasticity*, 20, (2004), 811–830.

Runkle, J.; Pelloux, R.: Micromechanisms of low-cycle fatigue in nickel-based superalloys at elevated temperatures. In: J. T. Fong, ed., *Fatigue mechanisms, proceedings of ASTM-NBS-NSF symposium, May 1978*, pages 501–527, American Society for Testing and Material, ASTM STP 675 (1979).

Sansoz, F.: *Propagation des petites fissures de fatigue dans les zones de concentration de contraintes dans le superalliage N18*. Ph.D. thesis, École Nationale Supérieure des Mines de Paris (2000).

Schirra, J.; Reynolds, P.; Huron, E.; Bain, K.; Mourer, D.: Effect of microstructure (and heat treatment) on 649° C properties of advanced P/M superalloy disk materials. In: K. A. Green; T. M. Pollock; H. Harada; T. E. Howson; R. C. Reed; J. J. Schirra; S. Walston, eds., *Proceedings of Superalloys 2004*, pages 341–350, TMS Warrendale USA (2004).

Shenoy, M.; Tjiptowidjojo, Y.; McDowell, D.: Microstructure sensitive modeling of polycrystalline IN100. *Int. J. Plasticity*, 24, (2008), 1694–1730.

Vattré, A.; Devincre, B.; Roos, A.: Dislocation dynamics simulations of precipitation hardening in Ni-based superalloys with high γ' volume fraction. *Intermetallics*, 17, (2009), 988–994.

Wendt, H.; Haasen, P.: Nucleation and growth of γ' precipitates in Ni14%Al. *Acta Metall.*, 31, (1983), 1649.

Wlodek, S. T.; Kelly, M.; Alden, D.: The structure of N18. In: S. D. Antolovitch; D. L. Anton; T. Khan; R. R. Kissinger; D. Klastrom; R. McKay; R. Stusrud, eds., *Proceedings of Superalloys 1992*, pages 467–476, TMS Warrendale USA (1992).

Address: Guylaine Boittin, Franck Gallerneau, Pascale Kanoute and Didier Locq, ONERA, DMSM, Châtillon Cedex, F-92322

Georges Cailletaud, Centre des materiaux, Mines ParisTech, CNRS/UMR 7633, Evry Cedex, F-91003

email: guylaine.boittin@onera.fr